RADIUS MEASUREMENTS FROM TIME-RESOLVED IMAGES OF A RELATIVISTIC ELECTRON BEAM

D. J. Weidman,[a] J. A. Antoniades, R. F. Fernsler, R. F. Hubbard,
D. P. Murphy, M. C. Myers, and R. A. Meger

Plasma Physics Division, Naval Research Laboratory
Washington, DC 20375-5346

Images of the cross-section of an intense relativistic electron beam are obtained using a fast framing camera called a Gated Optical Imager (GOI). Cherenkov radiation generated by the beam passing through a thin quartz plate is viewed by the GOI, which provides 2-ns resolution of the beam current density profile at three times during the beam pulse on each shot. These images have been characterized quantitatively to provide measurements of the electron beam radius and position, without assuming a particular form of the profile. Using a direct, pixel-by-pixel approach rather than an iterative technique to evaluate the image, the beam centroid and various measures of the radius are found, including for example finding all the contours and choosing one, such as the one that contains half the beam current. The algorithms that have been developed will be described, as well as the physical significance of the results, in terms of both a general profile and the electron beam in the experiment. These techniques may be applicable to quantitative measurements of the profile of any beam, such as a laser beam or an ion beam, and to the analysis of any two-dimensional image, such as the cross-section of a plasma.

These algorithms have been implemented for an experiment that studies beam propagation through the atmosphere.[1] Intense relativistic electron beams propagating through gas are subject to the resistive hose instability. The GOI is being used to study various "beam conditioning" techniques to reduce the effect of the hose instability and extend the propagation distance of the beam. The 5-MeV, 25-kA, 40-ns beam from SuperIBEX is injected into a 1-atm gas cell. Preliminary experimental results will be presented.

I. INTRODUCTION

This paper describes algorithms used to analyze two-dimensional images of the profile of a roughly circular electron beam and provide a measure of the beam radius; these algorithms were implemented on a personal computer. After describing the motivations for this work, the algorithms will be described in Section II, the analysis of computer-generated data will be examined in Section III, an electron beam experiment will be used as an example in Section IV, and a discussion will follow.

The data that are acquired in our experiment[1] consist of an image of an electron beam profile obtained by viewing a Cherenkov-light[2] emitter with a fast framing camera. The Cherenkov emitters that are used are 3-mil or 5-mil thick FEP film[3] or a set of 25-mil thick quartz plates next to each other to provide a large area. These are viewed through a 500-mm focal length telephoto lens or a 2-m telescope, depending on the area of the Cherenkov foil. A fast framing camera called a gated optical imager (GOI), which is operated at a "shutter speed" or gate time of only two nanoseconds, records the images. This system provides up to four images during the 40-ns beam.

A method of analyzing these images was developed that is as automated as possible. This method enables the data to be analyzed quickly and consistently, without the subjective judgements of an interactive system. A typical method that is chosen under such circumstances is curve fitting. The methods described here, however, have several advantages: they are easily implemented; they make no assumptions regarding the image profile, such as whether it can be modeled by a single-Gaussian or by a double-Gaussian curve; and because they are non-iterative, they are immune to possible convergence problems and can be faster. While the diagnostic used in this experiment, and the resulting data, is unique among beam propagation experiments, these algorithms may also be useful for analyzing time-integrated data or data from laser or plasma experiments.

As an example, data from an electron beam propagation experiment will be presented along with the results of analysis by these algorithms.

II. DESCRIPTON OF THE ALGORITHMS

Several measures of beam radius have been used. The definitions are given here, followed by an explanation of how these were implemented on a personal computer.

A. Definitions

Half-current contour: The half-current contour radius is defined here to be the radius of the circle that has the same area as the area enclosed by the contour that encloses half the current. "Current" is the sum of all the pixel values in the image, after correcting for background and assuming no saturation. This represents an unnormalized measure of the current of the electron beam. This definition has been used to try to measure beam profiles that may be slightly eccentric or filamentary without giving an unusually large radius value, as some of the other definitions discussed below may provide.

Half current-density contour: The half current-density contour radius is defined as the radius of the circle that has the same area as the area enclosed by the half current-density contour, which is that contour that has a value half of the maximum value of the image. Suppose the maximum pixel value of an image is 246. Then all pixels with values greater than 123 are considered to be within the half current-density contour. "Current-density" is used because each pixel value corresponds to the current-density of the electron beam profile that is measured in our experiment. Note that while the half-current contour is defined (above) by what it encloses, the half current-density contour is defined (here) by its value, regardless of what it encloses. An advantages of the half current-density contour radius is its ease of calculation: once the maximum pixel value of an image is found, it is straightforward to count how many pixels have a value greater than half of that.

Centroid and rms radius: The usual definitions of centroid and rms radius[4] are used here. The centroid $(\langle x\rangle, \langle y\rangle)$ is the weighted average position, or first moment, of the current density:

$$\langle x\rangle = \frac{\sum_i x_i j_i}{\sum_i j_i}, \text{ and} \tag{1a}$$

$$\langle y\rangle = \frac{\sum_i y_i j_i}{\sum_i j_i}. \tag{1b}$$

The centroid is the "balance point" of the image, in the sense that a plane with a mass density corresponding to the pixel intensities could be balanced by a single point only at the centroid. The rms (root mean squared) radius is the weighted average of the square of the position, or second moment and is given by $r_{\rm rms} = \sqrt{x_{\rm rms}^2 + y_{\rm rms}^2}$, where

$$x_{\rm rms} = \sqrt{\langle x^2\rangle} = \sqrt{\frac{\sum_i (x_i - \langle x\rangle)^2 j_i}{\sum_i j_i}}, \text{ and} \tag{2a}$$

$$y_{\rm rms} = \sqrt{\langle y^2\rangle} = \sqrt{\frac{\sum_i (y_i - \langle y\rangle)^2 j_i}{\sum_i j_i}}. \tag{2b}$$

An advantage of using the rms radius is the simplicity of calculation on a computer.

Contour centroid: The "contour centroid" is defined here to mean the centroid, as defined in Eq. (1), based on only those points within a certain contour. For example, if an image has a maximum value of 230, then the 10% contour centroid is the centroid calculated from only those pixels with a value of 23 or greater; all the other points, with smaller values, are ignored.

Contour rms radius: Similarly, the "contour rms radius" is defined here as the rms radius based on only those points within a certain contour; in order to make this consistent with the intention of including only certain parts of the image, the corresponding contour centroid is used. Continuing with the same example, the 10% contour rms radius would be the rms radius based only on those points with a value 23 or greater, using the values for the 10% contour centroid for $\langle x\rangle$ and $\langle y\rangle$ in Eq. (1).

The contour centroid definition was motivated by the presence of low level background light and the need for a measure of the beam position. Because of the weighting by x_i (or y_i) in Eq. (1), even low intensity light can have a large effect on the value of $\langle x\rangle$ (or $\langle y\rangle$) when it is near the edges of the image, especially if present over a large area.

Half-current circle radius: The half current circle radius is also determined. Although the above definitions use the word "radius," this is the only one that is based directly on a true circle and does not include any contours. The half current circle is the circle that is centered on the centroid and that encloses half the current. This was motivated by its conceptual simplicity and use in simulations, but may be more sensitive to variations in the beam profile than the other radius measurements.

Report Documentation Page

Form Approved
OMB No. 0704-0188

1. REPORT DATE	2. REPORT TYPE	3. DATES COVERED
JUN 1993	**N/A**	**-**

4. TITLE AND SUBTITLE	5a. CONTRACT NUMBER
Radius Measurements From Time-Resolved Images Of A Relativistic Electron Beam	5b. GRANT NUMBER
	5c. PROGRAM ELEMENT NUMBER
6. AUTHOR(S)	5d. PROJECT NUMBER
	5e. TASK NUMBER
	5f. WORK UNIT NUMBER
7. PERFORMING ORGANIZATION NAME(S) AND ADDRESS(ES) **Plasma Physics Division, Naval Research Laboratory Washington, DC 20375-5346**	8. PERFORMING ORGANIZATION REPORT NUMBER
9. SPONSORING/MONITORING AGENCY NAME(S) AND ADDRESS(ES)	10. SPONSOR/MONITOR'S ACRONYM(S)
	11. SPONSOR/MONITOR'S REPORT NUMBER(S)

12. DISTRIBUTION/AVAILABILITY STATEMENT
Approved for public release, distribution unlimited

13. SUPPLEMENTARY NOTES
See also ADM002371. 2013 IEEE Pulsed Power Conference, Digest of Technical Papers 1976-2013, and Abstracts of the 2013 IEEE International Conference on Plasma Science. Held in San Francisco, CA on 16-21 June 2013. U.S. Government or Federal Purpose Rights License.

14. ABSTRACT

15. SUBJECT TERMS

16. SECURITY CLASSIFICATION OF:			17. LIMITATION OF ABSTRACT	18. NUMBER OF PAGES	19a. NAME OF RESPONSIBLE PERSON
a. REPORT **unclassified**	b. ABSTRACT **unclassified**	c. THIS PAGE **unclassified**	**SAR**	**4**	

B. Implementation in computer code

Most of the radius definitions above use histograming[5] or binning of values to perform the calculations withing a reasonable amount of time. In our experiment, a fast framing camera system that produces images that are 704 by 528 pixels in size and these 371,712 pixels range in values from 0 to 255 (8-bit resolution). Once the values are binned, operations can be performed in one thousandth the amount of time that it would take to perform an operation on all the separate pixels of the original image.

The simplest example of binning is the half-current contour algorithm. A one-dimensional array p that has 256 elements is initialized with every element zero: $p_i = 0$. The image is scanned pixel by pixel. As each pixel is read, the element of the array that corresponds to the pixel intensity is incremented by one. For example, if the array elements are numbered 0 through 255, and the first pixel has a value of 3, then element three of the array, p_3, is incremented by one. This is repeated for every pixel of the image. Further operations are performed on the values in the array and are much quicker than operations on all the pixel values of the image. For the half-current contour calculation, the elements of the array are each multiplied by the pixel value that they represent and added one by one until half of the current (i.e., half of the sum of the pixel values $\Sigma_{i=0}^{255} i p_i/2$) is reached: $255p_{255} + 254p_{254} + 253p_{253} + \ldots + i_{\text{half}} p_{i_{\text{half}}}$. The number of pixels that have been counted is: $N = \Sigma_{i=i_{\text{half}}}^{255} p_i$. The area A covered by these pixels is N times the area per pixel, which depends on the magnification of the optics. The half-current contour radius is then $\sqrt{A/\pi}$.

Another example of binning the data into an array is the method used to determine the half-current density contour radius. At first, it may seem that the entire image must be examined pixel by pixel to determine the maximum pixel value, and then examined a second time to determine which points are above the half-current-density (half-maximum-pixel-value) contour. Only one pass, however, is necessary, if each pixel value is binned as described above for the half-current contour radius. The maximum pixel value $i_{\max}$ of an unsaturated image might be 242, for example. The pixel value that represents the half-current-density contour i_{half} would then be 121. The number of pixels that have intensity values between 121 and 242 are then counted, and then the area A can be determined as described above. Since examining each pixel of the image before binning is the most time-consuming step, this technique can almost halve calculation time.

The way the contour centroid is determined is a good example of how the binning concept can be extended to less obvious possibilities than those described above. We typically find ten centroid values: the centroid based on all the points (i.e., those above 0% intensity of the maximum pixel value), the centroid based on the 10% points (those above 10% of the maximum pixel value), the one based on the 20% points, 30%, ..., and 90%. This can be done with a two-dimensional array of size 2×256 in which the values of $x_i j_i$ and $y_i j_i$ are stored. Then, the appropriate range of elements of this array are summed [to obtain the numerator in Eq. (1)] and divided by the sum of the appropriate range of elements of the arrays discussed above [to obtain the denominator of Eq. (1)]. The "appropriate range" is determined by the contour centroid that is being found, e.g. the 20%-contour centroid. Note that this technique allows binning of the information on a single pass of reading the image.

Finding the contour rms radius is a good example of how the binning technique can be further extended. The rms radius depends on the centroid [Eq. (1)], but all the contour rms radii can be calculated with only one additional pass through the array of pixels that represent the image. Suppose the ten contour rms radii that correspond to the ten contour centroids described above are to be calculated. During the additional pass, ten additional pairs of values are summed, representing the numerators of Eq. (1); only those values that have an intensity larger than the appropriate value (e.g., 20% of the maximum pixel value and above) are counted in each sum. (What is actually done, for slightly improved speed, is to sort these values into ten bins and then add the values later. Each bin has the values of those bins above it added to it.)

The half-current circle radius is determined by finding the circle centered on the centroid that encloses half the current. This is the only definition that directly relates an actual circle to the image. The way the half-current circle is found is that the size of an initial circle is increased slightly, the newly enclosed pixels are added, and this process is repeated until half the current is enclosed; this technique has been used before for analyzing laser-beam profiles.[6] In order to speed up calculation time, we choose as the initial circle the one with a radius equal to the half the length of a side of the half-current square, which is relatively quick to determine; this is the square centered on the centroid that encloses half the current. The half-current-circle radius will have a value between the half-current-square half-edge $s/2$, which is half the length of a side, and the half-current-square half-diagonal $s/\sqrt{2}$: $s/2 < r < s/\sqrt{2}$, as shown in Fig. 1.

The half-current circle is found fairly efficiently if a couple of simple techniques are used. Only one quadrant is examined to test whether a pixel is inside the circle or not, that is whether $x_i^2 + y_i^2 < r^2$, and then it is immediately known, by symmetry, whether to count the corresponding

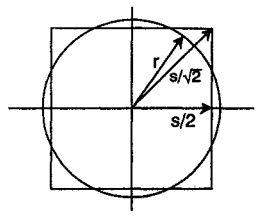

Fig. 1. The half-current square can be found quickly. If the side is length s, then the diagonal has length $s\sqrt{2}$ and the half-current-circle radius r is known to be in the range $s/2 < r < s/\sqrt{2}$.

points, $(-x_i, y_i)$, $(-x_i, -y_i)$, and $(x_i, -y_i)$, in the other three quadrants. Also, since a running total is kept while only increasing the radius, pixels that have already been included are not examined repeatedly as to whether they are inside the circle. If the pixels are square and the scale is the same in both the x and y directions, then an even faster technique could be used in which pixels are added up starting at the origin and expanding outward in a predetermined pattern corresponding to the order of pixels according to the distance from the origin.

III. EXAMINATION OF COMPUTER-GENERATED DATA

Several ideal functions were used for testing the algorithms. Such tests help verify the algorithms and shed light on how the algorithms work. These tests also demonstrate various effects encountered in the experiment, such as the finite field-of-view and a uniform background level.

A. Analytic form of functions

This section presents the a few functions in the form that they are used in this paper.

A Gaussian curve is used of the form

$$j = \frac{I}{\pi a^2} e^{-r^2/a^2}, \tag{3}$$

so that I is the total current, which is defined as

$$I \equiv \int_{r=0}^{\infty} \int_{\theta=0}^{2\pi} j(r)\, dA, \tag{4}$$

where $dA = r dr d\theta$, and a, which is the Gaussian radius, represents the rms radius in two dimensions, if the rms value of any parameter f for a distribution j in two dimensions is defined as

$$\sqrt{\langle f^2 \rangle} \equiv \left[\frac{\int_{r=0}^{\infty} \int_{\theta=0}^{2\pi} f^2\, j(r)\, dA}{\int_{r=0}^{\infty} \int_{\theta=0}^{2\pi} j(r)\, dA} \right]^{1/2} \tag{5}$$

Although the half-current radius r_{hc} cannot be written explicitly in general, it is defined for a distribution that is independent of θ by the equation

$$\frac{I}{2} = 2\pi \int_{r=0}^{r_{\text{hc}}} j\, r dr. \tag{6}$$

The half-current-density radius r_{hcd} also cannot be written explicitly, but is defined for a distribution that is independent of θ by the equation

$$\frac{j(r=0)}{2} = j(r_{\text{hcd}}), \tag{7}$$

where the left hand side can be expressed as $j_{\max}/2$ or $I/(2\pi a^2)$.

Note that for a Gaussian, $r_{\text{hc}} = r_{\text{hcd}}$, which is verified by substituting Eq. (3) into Eqs. (6) and (7). Also, when solving Eq. (6) for r_{hc} or Eq. (7) for r_{hcd}, it is found that $r_{\text{hc}} = r_{\text{hcd}} = a\sqrt{\ln 2} = 0.833a$.

A Bennett distribution[7] is an equilibrium for an electron beam propagating through gas and is given by the form

$$j = \frac{I}{\pi a^2} \left[\frac{1}{1 + (r/a)^2} \right]^2, \tag{9}$$

where a is the Bennett radius. Since substituting Eq. (9) into Eq. (5) does not provide a finite value, the rms radius of a Bennett profile does not exist, because the distribution falls off with r too slowly. The

half-current radius, the Bennett radius, and the quarter-current-density radius all are equal to each other. The half-current-density radius is $0.644a$.

A flattop or square profile is given by

$$j = \frac{I}{\pi a^2}\left[1 - H(r-a)\right], \tag{10}$$

where H is the unit step function defined by the equations $H(x<0)=0$ and $H(x>0)=1$, so that $j = I/\pi a^2$ for $r < a$ and $j = 0$ for $r > a$. I is the volume under the surface. The rms radius and the half-current radius are both $a/\sqrt{2}$. The half-current-density radius and the quarter-current density radius are a.

B. Computer-generated data

The above ideal functions were analyzed using the algorithms described in Section II. A 1 cm ($a = 1$) Gaussian image 100×100 pixels (px), 15 px/cm in both x and y, was analyzed yielding a half-current radius of 0.8385 cm, which is within 1% agreement of the ideal value of 0.8326 cm. The half-current-density radius is 0.8317 cm, the rms radius is 0.9955 cm, and the half-current circle radius is 1.0 cm, which are also within 1% of their ideal values.

If a uniform background is present, the level is determined by sampling a small area in the corner of the image and it is subtracted before any calculations. This works well for an image with these parameters, because the Gaussian falls off quickly to a negligible value. If the peak value of the Gaussian is 200, and saturation occurs at 255, a uniform background up to 55 has no effect. A background level of up to about 80 can be tolerated with results still within 10%. In this case, the portion of the original Gaussian above 175 is saturated.

A 1 cm Bennett profile with the same image parameters as above of 100×100 px, 15 px/cm, 1 cm radius, and no background was also analyzed. The half-current radius is 0.897 cm, which has an error of about 10%, the quarter-current-density radius is 0.993 cm (<1% error), and the half-current circle radius is 1.07 cm (7% error). The source of this error is that, as shown in Fig. 2, a Bennett distribution is broader than a Gaussian and the "wings" are more easily cut off. Since the width and height of the entire image are 6.67 cm, the ratio of the image half-width to the Bennett radius is 3.3. When this ratio is above 4, the error drops to below 2%. Note that the quarter-current-density contour radius is unaffected by this spatial cutoff.

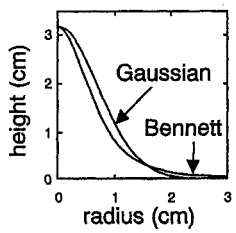

Fig. 2. A Gaussian and a Bennett profile, both with 1 cm radius and volume 10 cm^2 [$a = 1$ and $I = 10$ in Eqs. (3) and (9)]. Note that for $r > 1.585$, more volume is under the Bennett than under the Gaussian.

A 1 cm flattop profile with the same image parameters as the above two cases provided interesting results. The rms radius was calculated to be 0.7022 cm, which agrees well with the ideal value 0.7071 cm. The algorithm that normally produces the half-current radius, however, results in a 100%-current radius of 0.993 cm, because after binning the values in the 256-element array, there are values in only one bin, and when stepping to include more and more current, all the current is counted at once. When noise is simulated, this problem is diminished because of the presence of data in several of the elements of the array.

IV. ELECTRON BEAM EXPERIMENT

A. Brief overview of beam experiment

The intense relativistic electron beam research being conducted at the Naval Research Laboratory is concerned with long-range propagation through the atmosphere. The 5 MeV, 25 kA, 40 ns electron beam produced by the SuperIBEX machine is "conditioned" by one or more of the following cells: a small-diameter ion-focused regime (IFR) centering cell, a large-diameter IFR cell for radius tailoring, and a gas-filled or vacuum B_θ cell for centering, aiming, and conditioning. A material that will produce Cherenkov light[2] is placed in the path of the beam. Cherenkov light is produced when the electron velocity v_e is greater than the phase velocity of light in the material c/n, where c is the velocity of light in vacuum and n is the index of refraction of the material. The choice of material depends on the light-production efficiency that is needed, which depends on the beam current and on the sensitivity of the optical diagnostics. Typically, for electron-beam current-densities on the order of 1 kA/cm^2, a thin sheet of FEP film[3] is used. This allows beam propagation after the foil without significant beam temperature (or emittance) increase. If the beam current-density is much lower, then the quartz plates are used, but then the beam is heated significantly and quickly expands after passing through the quartz. The light from the FEP film is bounced off two mirrors, focused by a telescope, and split into four images,[8] as shown in Fig. 3. Each of the four images is captured by a gated CCD camera, which is read out by a frame grabber. After each shot, the image from each of the four frame grabbers is uploaded to a Macintosh computer as TIFF[9] (tagged image-file format) files. For convenience when analyzing data, an application was written that runs under Microsoft[10] Windows that reads the TIFF files directly, performs the algorithms on up to four images, and writes a text file for each image summarizing the results.

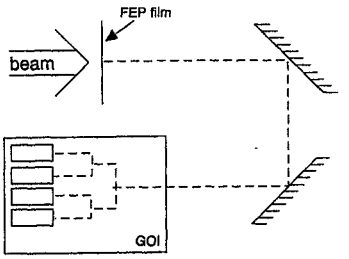

Fig. 3. Schematic of the experiment showing the electron beam, FEP film, light path, and the GOI.

B. Experimental considerations regarding these alorithms

There are several experimental factors to consider regarding the algorithms.

Separate x and y scales are allowed in the algorithms because viewing was often done at an angle rather than directly end on, as shown in Fig. 4, and the pixels of an image that is being analyzed may not be exactly square. Viewing at the Cherenkov angle was not essential because the downstream surface of the material was roughened, scattering the light so uniformly that the light intensity at the camera was almost independent of the viewing angle.

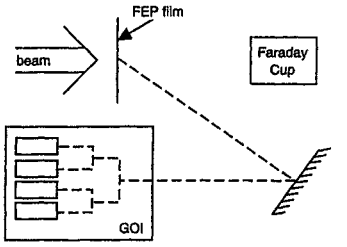

Fig. 4. Viewing the Cherenkov foil at an angle allows another diagnostic to be used, such as a Faraday cup.

The dependence of the pixel value on the parameter of interest may or may not be linear. In our case, it is convenient that the Cherenkov light is linear with current density. That the light is Cherenkov light has been confirmed by verifying that it has a prompt rise, a prompt decay, and a blue color. The rise and decay times were measured using the GOI and the color was viewed with an open-shutter camera. Also, the frame grabbers were adjusted to have a linear response. If a system is used that provides pixel values that are nonlinear with the parameter of interest, because of the response of the detector, optics, or camera system, then a correction must be made at some point during the calculations. Remapping the data may be done most easily after binning, when there are only 256 separate values rather than when there are as many values as there are pixels in the image.

Saturation is always avoided when collecting the data, because it cannot be handled by these algorithms. Each of the four cameras has an independent gain adjustment to allow saturation to be avoided.

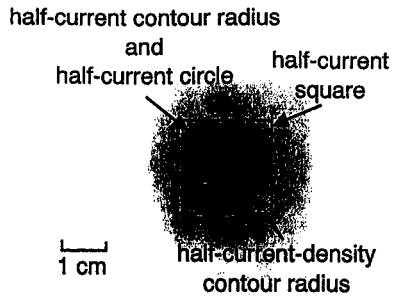

Fig. 5. A typical image from an experiment of the time-resolved cross-section of an electron beam.

Threshold is not a concern because it is a small effect. Ideally, it would be 1 part in 256, or 0.4 %, for an 8-bit system. In practice, it is typically a few parts in about 200, or a few percent.

C. Experimental results

Figure 5 shows a typical image (Shot 1635, Frame 1) from the experiment, with black and white reversed. The circle labeled "half-current contour radius" has a 1.09 cm radius and is the circle that has the same area as the contour that encloses half the current. In this case, this contour is the set of points with a value of 40% of the peak value. The circle labeled "half-current-density contour radius" has a radius of 0.933 cm and is the circle that has the same area as the 50% contour. The half-current square has an edge of length 1.98 cm and the half-current circle has a radius of 1.16 cm. Because the image is so circular and falls off monotonically with radius, the half-current circle radius is almost as small as the half-current contour radius. Note that the half-current square and half-current circle intersect in Fig. 5 as described in Fig. 1. Figures 6 and 7 show the data from the same image as Fig. 5. The outer bold contour is the 40% contour and the inner bold contour is the 50% contour.

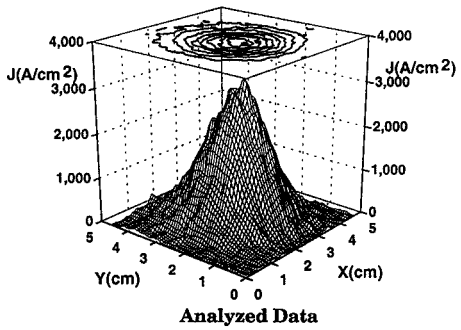

Fig. 6. Plot of pixel value intensity of the image in Fig. 5.

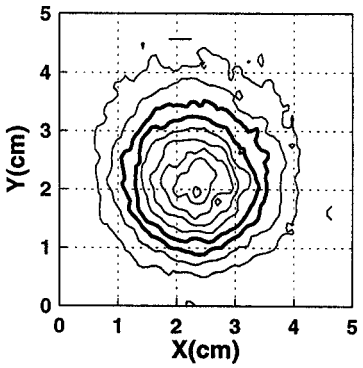

Fig. 7. Contour plot of the image in Fig. 5. The outer bold contour is the 40% contour and the inner bold contour is the 50% contour.

As an example of how these algorithms have been useful in an experiment, Fig. 8 shows a plot of the position of the 20%-contour centroid from several shots. Each shot has up to four images. The centroid based on the points within the 20% contour was chosen because this automatically ignores low intensity values that may be noise and that affect the centroid calculation. An estimate of the eccentricity is based on the rms x and rms y measurements of Eq. (2) and is zero for a circular image. The eccentricity based on all the points is relatively large because for these rectangular fields-of-view, the faint background causes a larger value to be calculated for the rms x value. The eccentricity is significantly smaller when based on those points with intensity of 20% of the peak or higher, and, therefore, the 20% centroid is taken as a more accurate measure of beam position than the centroid based on all points.

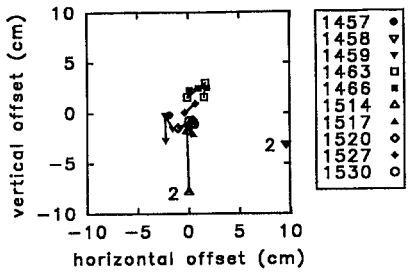

Fig. 8. Example of experimental results: the position of the 20%-contour centroid for several shots.

V. DISCUSSION

We have described algorithms for determining the radius of an image that represents the cross-section of a beam. There are several definitions of radius, and each one is relatively easy to implement on a personal computer. Many of these definitions can be easily modified, if desired. For example, instead of the half-current contour or half-current circle, the 90%-current contour or 90%-current circle could be used. By analyzing computer-generated data with known parameters, we have verified the algorithms and also studied various experimental effects such as a finite field-of-view and saturation. Experimental data was shown as an example of the way in which some of these algorithms can be used.

VI. ACKNOWLEDGMENTS

We would like to thank S. Slinker for his help with the half-current circle algorithm. We would also like to thank G. W. Littlejohn of Saks Freeman Associates and A. K. Noll for their technical assistance with the electron beam experiment. This work was supported by the Office of Naval Research.

VII. REFERENCES

a) Laboratory for Plasma Research, University of Maryland, College Park, Maryland 20742

[1] See National Technical Information Service (NTIS) Document No. PB92-206168, R. A. Meger, R. F. Hubbard, J. A. Antoniades, R. F. Fernsler, M. Lampe, D. P. Murphy, M. C. Myers, R. E. Pechacek, T. A. Peyser, J. Santos, and S. P. Slinker, *Proceedings of the 9th International Conference on High Power Particle Beams*, edited by D. Mosher, G. Cooperstein, and V. Granatstein, Washington, DC, May 1992. Copies may be ordered from the NTIS, Springfield, VA 22161.

[3] FEP (fluorinated ethylpropylene) film is sold by E. I. duPont de Nemours & Co. Inc. as FEP "Teflon," which is a registered trademark.

[4] W. H. Beyer, ed., *CRC Standard Mathematical Tables, 26th Ed.*, (CRC Press, Inc., Boca Raton, Florida, 1981), for example.

[5] R. A. Schowengerdt, *Techniques for Image Processing and Classification in Remote Sensing*, (Academic Press, Inc., New York, 1983), and A. Rosenfeld, "Image Analysis," in *Digital Image Processing Techniques*, edited by M. P. Ekstrom, (Academic Press, Inc., New York, 1984), for example.

[6] J. D. Frank, Opt. Eng. **25**, 132 (1986).

[7] W. H. Bennett, Phys. Rev. **45**, 890 (1934), and W. H. Bennett, Phys. Rev. **98**, 1584 (1955).

[8] D. P. Murphy, T. A. Peyser, and R. E. Pechacek, Naval Research Laboratory Memorandum Report 6754-93-7322, (May 26, 1993).

[9] C. A. Lindley, *Practical Image Processing in C: Acquisition, Manipulation, and Storage*, (John Wiley & Sons, Inc., New York, 1991), for example.

[10] "Microsoft" is a registered trademark of Microsoft Corporation.